Urban Land Cover Classification With Airborne Hyperspectral Data: What Features to Use?

Xiaohua Tong, Huan Xie, and Qihao Weng

***Abstract*—This paper investigates the potential effects of spectral, shape, textural, and height information and their combinations on the classification of urban areas using airborne hyperspectral data. Based on analysis of the spectral, shape, textural, and height characteristics of urban land covers, the first ten spectral principal components, eight shape components, one height component, and seven textural components were selected to examine their performance on the classification accuracy. Correlation analysis was conducted to exclude correlated components. A support vector machine (SVM) was employed to determine the significant components affecting the urban hyperspectral classification through comparison of the classification accuracy. Different combinations of these components were then tested to estimate their contributes. The classification results showed that all these components contribute to the result of urban land cover classification, but different land cover classes benefit from the inclusion of different components. The experiment further revealed the effect of significant components on the classification of urban land cover in terms of area, convexity, elongation, form factor, rectangular fit, roundness, textual factors, and mean relative height. It is suggested that the inclusion of shape, texture, and height, together with the spectral components, significantly improved the classification accuracy of urban land cover.**

***Index Terms*—Classification accuracy, hyperspectral imagery, support vector machine (SVM), urban land cover.**

I. Introduction

URBAN land cover types and their areal distributions are fundamental data required for a wide range of environmental and socioeconomic applications [1]–[4]. With the dynamic development of urban areas, there is an increasing need for automatic identification of urban land cover types. Comparing with traditional approaches of updating urban land cover, such as field measurements, remote sensing is an attractive approach for determining urban land cover since it provides a map-like representation of the Earth's surface that is spatially continuous and highly consistent, and it can be carried out in a range of spatial and temporal scales [5]. One of the frequently employed methods for thematically mapping urban land cover is image classification of remotely sensed data [5]. Remotely sensed data have spectral, spatial, textural, and other characteristics [6]. As a result, a key concern in image classification is to investigate significant remote-sensing components describing spectral, shape, textural, and height features of urban surface materials and to determine how they affect the classification result [7].

For medium-resolution remote sensing data, such as Landsat thematic mapper (TM), spectral information is the most important information in image classification [8]–[12]. For sensors with higher spatial resolution, such as SPOT, ETM+ and ASTER, texture and spatial features, together with spectral ones, have shown to be the important components in urban classification [6], [14]–[21]. Fine spatial resolution data (e.g., better than 5-m spatial resolution), such as IKONOS and QuickBird data, have been increasingly adopted in urban studies, providing the potential to extract much more detailed information about urban surface materials than medium spatial resolution data. Therefore, much attention has shifted toward developing object-based classification algorithms using geometric features, rather than the traditional per-pixel classification algorithms using spectral features, in urban land cover classification [22]–[25]. Recently, the incorporation of features from other data sources, such as height information from digital surface models (DSMs), in image classification, has been reported for improving classification accuracy [11], [12], [26]–[29]. In several previous studies, shape, texture, and height features, obtained from either the images or other data sources, have been shown useful for image classification [30]–[32].

As far as the detailed mapping of urban areas is concerned, airborne hyperspectral remote sensing, as characterized by very high spatial and spectral resolutions [33], [34], is one of the most valuable data sources for classification [35]. In such mapping applications, spectral information is certainly an important feature since urban surface materials have high dimensionality in the spectral space [36], [37]. However, about the separation of urban surface materials based on spectral characteristics is often inadequate [38]. In addition to the wide diversity of urban surface materials, better knowledge about spatial–temporal changes in urban land cover is equally important in determining and modeling urban environmental conditions [14], [39], [40].

Manuscript received August 31, 2012; revised January 14, 2013 and February 26, 2013; accepted March 28, 2013. Date of publication July 23, 2013; date of current version December 22, 2014. This work was supported by the National Natural Science Foundation of China (Project Nos. 41201426 and 41171352), National Key Basic Research Program of China (973 Program) (Project No. 2012CB957701), Fund of the Doctoral Program of Higher Education (Project No. 20110072120066), and Fund of Shanghai Municipal Education Commission and Shanghai Outstanding Academic Leaders Program (Project Nos. 11CG21 and 12XD1404900).

X. Tong and H. Xie are with the College of Surveying and Geo-Informatics and UNEP–Tongji Institute of Environment for Sustainable Development, Tongji University, Shanghai 200092, China (e-mail: xhtong@tongji.edu.cn; huanxie@tongji.edu.cn).

Q. Weng is with the Center for Urban and Environmental Change, Department of Earth and Environmental Systems, Indiana State University, Terre Haute, IN 47809 USA (e-mail: qweng@indstate.edu).

Color versions of one or more of the figures in this paper are available online at http://ieeexplore.ieee.org.

Digital Object Identifier 10.1109/JSTARS.2013.2272212

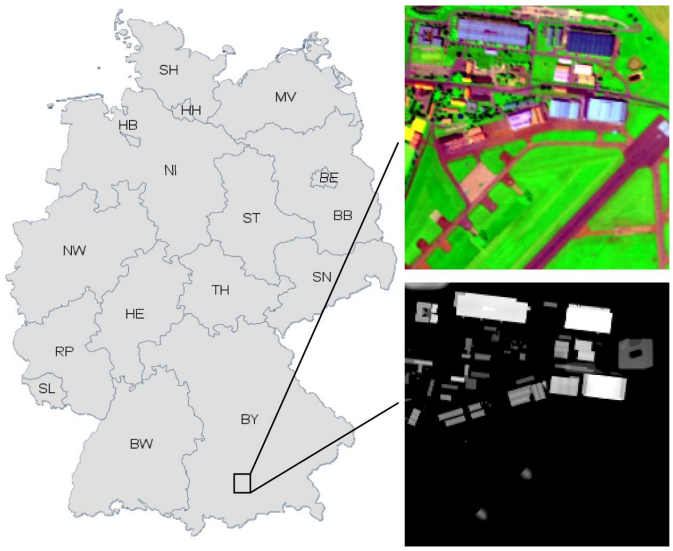

Fig. 1. Study area one: Oberpfaffenhofen, Bayern, Germany (upper: the false color HyMap image; lower: the normalized DSM).

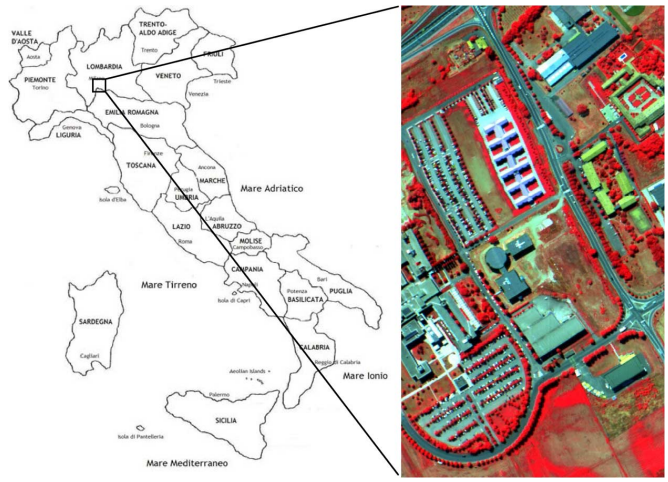

Fig. 2. Study area two: Pavia, Lombardy, Italy.

As a result, much effort has been made to improve urban classification of airborne hyperspectral images by using spectral, shape, and textural information. This feature information includes, for example, census data [41], LiDAR information on the surface structure [42], and texture measures such as the extended morphological profiles [43]. Making full use of remote sensing information may be the most efficient and effective way to improve classification accuracy [44]. However, little attention has been paid to the comprehensive determination and evaluation of significant remote-sensing components, including spectral, spatial, textural information, as well as height information from additional data sources, in terms of the hyperspectral classification of urban land covers.

Therefore, the objectives of this paper are 1) to investigate the potentials of spectral, shape, and textural information from airborne hyperspectral data, as well as relative height information from a DSM, in improving the classification accuracy of urban land cover, and 2) to identify the most significant remote-sensing components from a set of spectral, shape, textural, and height features for urban land cover classification.

II. Data and Study Areas

In our study, two comprehensive experiments were conducted using two kinds of airborne hyperspectral images in different study areas.

Study area one (Fig. 1) is situated in Starnberg, Oberbayern, Bayern, Germany, with central geographical coordinates of $48°4'$ N and $11°16'$ E. The hyperspectral data of this study area were recorded by the airborne hyperspectral mapper (HyMap) system on June 7, 2004. The image data are provided in 126 spectral bands with a spatial resolution of 4 m. Detailed information about the HyMap sensor was given by [45]. The DSM, however, was manually created from a pair of stereo aerial photographs. In the study, both the DSM and HyMap image cover an area of approximately 0.64 km^2.

Study area two (Fig. 2) is located in Pavia, Lombardia, Italy. The dataset was acquired from the Reflective Optics System Imaging Spectrometer (ROSIS) sensor, with 103 spectral bands and a spatial resolution of 1.3 m, during a flight campaign over Pavia, northern Italy, with central geographical coordinates of $45°11'$ N and $9°9'$ E on July 8, 2002. The image covers an area of approximately 0.35 km^2. Detailed information about the ROSIS sensor can be seen in [46].

From Figs. 1 and 2, it can be observed that the land cover classes in these two study areas are primarily buildings, roads, and vegetation. A thorough analysis of the land cover classes in the two study areas is discussed in detail in the following section.

III. Methods

A. Framework of the Study

Fig. 3 shows the entire framework of the study. There are three main parts to the study: 1) characteristic analysis of urban land cover classes; 2) data preprocessing for extraction of the remote-sensing components; and 3) determination and evaluation of the significant components that affects most the classification result. In addition, the height information is only available for Study area one in the following analysis.

1) Characteristic Analysis of Urban Land Cover Classes: To investigate the potential components affecting the hyperspectral classification, characteristic analysis of urban land covers in the study areas was carried out as follows. 1) The spectral characteristics of urban surface materials in the reflective wavelength range were first examined, and the urban land cover were therefore subdivided into thematically and spectrally meaningful categories. 2) Eight shape components and seven co-occurrence textural components in the airborne hyperspectral image were selected for urban land cover classification. 3) The height component, derived from the DSM model as an additional source of information, is combined with the other components for better separation of certain urban land cover types, such as buildings and open spaces.

2) Data Preprocessing: Generally, there are four steps in preprocessing the hyperspectral imagery and DSM data used in the experiments: 1) correcting the geometric, radiometric and atmospheric errors in the hyperspectral images; 2) creating the dig-

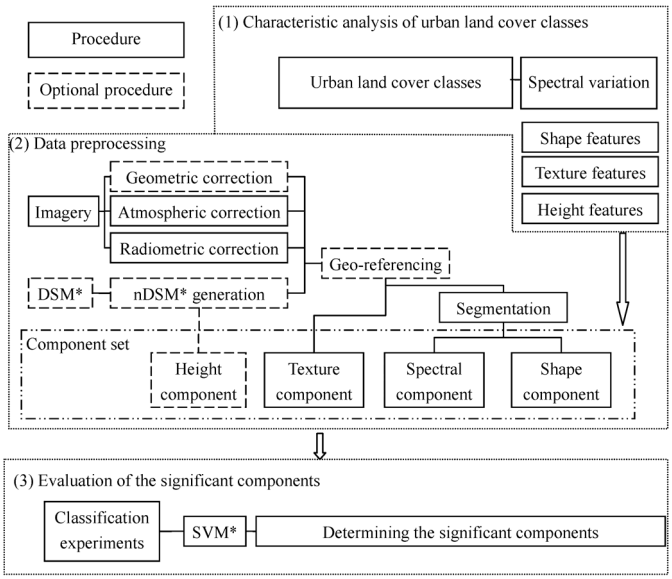

Fig. 3. Overall technological framework of the study.

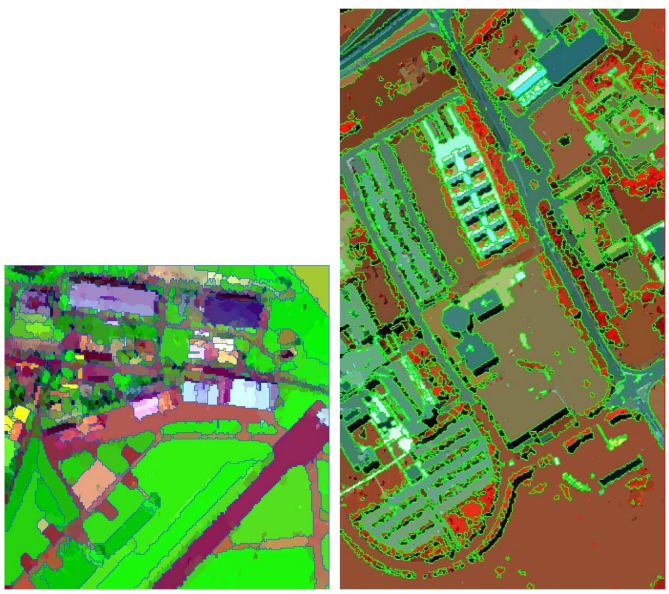

Fig. 4. Segmentation results in study areas 1 and 2.

ital terrain model (DTM) from the DSM by filtering building objects and producing the normalized DSM (nDSM) by differencing the DSM and DTM (this data is only available for Study area one); 3) generating the image segments [47], [48] and calculating the mean spectrum of each segment representing the region's spectral characteristic; and 4) computing the shape, textural, and height components in each segment. Fig. 4 shows the segmentation results in both study areas 1 and 2.

3) Evaluation of the Significant Component Set: In the study, support vector machine (SVM) classification method is used in the evaluation of the significant remote-sensing components, and two cases are designed: 1) classification with the spectral component only, and 2) classification with a combination of the spectral component and one additional component from the set of shape, textural, and height features. In the experiment, each of these components is input as an individual band in the airborne hyperspectral data classification, and the contribution of each component is evaluated separately in terms of accuracy improvement in the classification.

B. Quantitative Features of Urban Land Cover Classes

This section analyzes the characteristics of the spectral, shape, textural, and height features of urban land cover types in the study areas. This is the basis for the subsequent automated classification.

1) Spectral Characteristics of the Airborne Hyperspectral Imagery: Specifically, in study areas 1 and 2, the urban land cover types are subdivided into thematically and spectrally meaningful categories. In study area 1, vegetation areas consist of tree/bushes and lawn, and built-up areas consist of roofs, open spaces, tennis courts, and roads. Further, in study area 2, vegetation areas consist of tree/bushes and lawn, and built-up areas consist of roofs, open spaces, roads, and shadow.

Furthermore, the vegetated areas in Figs. 1 and 2 can be clearly differentiated from the built-up areas owing to the strong reflection of chlorophyll in the near-infrared. However, some urban surface classes containing similar materials, particularly in study area 1, such as precast concrete roofs and concrete open spaces, are difficult to spectrally differentiate from the image spectra. Another challenge arises from the spectral similarities of roads and roofs, and open spaces and roads.

2) Shape Characteristics of the Urban Land Cover: Over recent years, shape characteristics have been successfully used in image classification [49], [50]. In our experiment, eight candidate shape components are used: area (A), compactness (C), solidity (S), rectangular fit (RF), roundness (R), convexity (CX), form factor (F), and elongation (E) [51].

Area (A): In non-georeferenced data, the area of a single pixel is 1. Consequently, the area A of an image object is the number of pixels it contains. If the image data are georeferenced, then the area of an image object is the area covered by one pixel times the numbers of pixels forming the image object.

Compactness (C): Compactness represents how compact a region is and is defined as $C = \sqrt{4A/\pi}/\text{outer contour length}$, where A is the area of the object, and *out contour length* is the sum of the lengths of the outer edges of the polygon representing the image region (the edges of holes are excluded). A circle is the most compact shape with a compactness value of $1/\pi$, and the compactness value of a square is $C = (1/2)\sqrt{\pi}$.

Solidity (S): Solidity is the ratio of the area of the polygon to the area of a convex hull surrounding the polygon, and is calculated by $S = A/\text{area of convex hull}$, where A is the area of the object, and *area of convex hull* is the area of the smallest convex set containing the image region. The solidity for a convex polygon with no holes is 1.0, and the value for a concave polygon is less than 1.0.

Rectangular Fit (RF): Rectangular fit indicates how well the shape is described by a rectangle, which is expressed by $RF = A/\text{Max}L * \text{Min}L$, where A is the area of the object, and $\text{Max}L$ and $\text{Min}L$ are the lengths of the major and minor axes, respectively. Both axes are derived from an oriented bounding box containing the object. The rectangular fit for a rectangle is 1.0, and the value for a nonrectangular shape is less than 1.0.

Roundness (R): Roundness compares the area of the polygon with the square of $\mathrm{Max}L$. The roundness for a circle is 1, and the value for a square is $4/\pi$. The roundness is computed by $R = 4A/\pi \mathrm{Max}L^2$.

Convexity (CX): Convexity measures the convexity of the polygon, and is represented by CX = length of convex hull combined length of all boundaries of the polygon, where *length of convex hull* is the total length of the smallest convex set containing the image region, and *combined length of all boundaries of the polygon* is the sum of the lengths of all edges of the polygon representing the image region (edges of holes are included). The convexity for a convex polygon with no holes is 1.0, while the value for a concave polygon is less than 1.0.

Form Factor (F): The form factor compares the area of the polygon with the square of the total perimeter. The form factor of a circle is 1, and the value for a square is $\pi/4$. The form factor is calculated by $F = 4\pi A/(\text{total perimeter})^2$.

Elongation (E): Elongation measures the length of the image region, and is defined as $E = \mathrm{Max}L/\mathrm{Min}L$, where $\mathrm{Max}L$ and $\mathrm{Min}L$ are the lengths of the major and minor axes. The elongation for a square is 1.0, and the value for a rectangle is greater than 1.0.

In the above-mentioned eight shape components, the parameters used in the latter seven ones, e.g. *out contour length*, *area of convex hull*, $\mathrm{Min}L$, $\mathrm{Max}L$, and *total perimeter*, are related to the first one *Area*. Therefore, the component *Area* (A in the above equations) is accounted for in the calculation of the rest seven components. As a result, the values of these seven factors (i.e., *compactness (C)*, *solidity (S)*, *rectangular fit (RF)*, *roundness (R)*, *convexity (CX)*, *form factor (F)* and *elongation (E)*) range from 0 to 1.

3) Texture Characteristics of Urban Land Cover: In our experiments, the gray-level co-occurrence matrix (GLCM) was used to describe image texture. In GLCM calculation, a window with a size of 20 m × 20 m, corresponding to 5 pixels × 5 pixels in study area 1 and 15 pixels × 15 pixels in study area 2, was used. This window size represents approximately the average distance between urban land-cover objects, which was identified by the spatial autocorrelation analysis [36]. In the experiment, seven candidate texture descriptors were examined, including energy, entropy, contrast, correlation, variance, dissimilarity, and homogeneity [52], [53].

Energy (ene): Energy measures texture uniformity, or pixel pair repetitions. High energy occurs when the distribution of gray level values is constant or period. Thus, energy is defined as $ene = \sum_{i=0}^{N_g-1}\sum_{j=0}^{N_g-1} g^2(i,j)$, where $g(i,j)$ is the (i,j)th entry in GLCM and $g(i,j) = p(i,j)/\sum_{i=0}^{N_g-1}\sum_{j=0}^{N_g-1} p(i,j)$, $p(i,j)$ is the occurrence of gray levels i and j, as measured at two pixels separated by a given displacement vector, and N_g is the number of gray levels of the image.

Entropy (ent): Entropy measures the disorder of an image. Entropy is high when the texture is not uniform within the image and is defined as $\mathrm{ent} = \sum_{i=0}^{N_g-1}\sum_{j=0}^{N_g-1} g(i,j)\cdot\log(g(i,j))$.

Contrast (con): Contrast measures the difference between the highest and lowest values of a contiguous set of pixels. Low contrast image features low spatial frequencies, and contrast is defined as $\mathrm{con} = \sum_{i=0}^{N_g-1}\sum_{j=0}^{N_g-1}(i-j)^2\cdot g(i,j)$.

Variance (var): Variance is a measure of heterogeneity. It increases when the gray level values differ from their mean and is defined as $\mathrm{var} = \sum_{i=0}^{N_g-1}\sum_{j=0}^{N_g-1}(i-u)^2\cdot g(i,j)$, where $u = \sum_{i=0}^{N_g-1}\sum_{j=0}^{N_g-1} i\cdot g(i,j)$.

Correlation (cor): Correlation is a measure of gray tone linear dependencies in the image. High correlation values imply a linear relationship between the gray levels of pixel pairs, and correlation is defined as $\mathrm{cor} = \sum_{i=0}^{N_g-1}\sum_{j=0}^{N_g-1}(i-u)\cdot(j-u)\cdot g(i,j)/\sigma^2$, where $\sigma^2 = \sum_{i=0}^{N_g-1}\sum_{j=0}^{N_g-1}(i-u)^2\cdot g(i,j)$.

Dissimilarity (dis): The dissimilarity is similar to *contrast*. Instead of weighting the diagonal quadratically, the dissimilarity weights increase linearly. Thus, it is calculated by $\mathrm{dis} = \sum_{i=0}^{N_g-1}\sum_{j=0}^{N_g-1} g(i,j)|i-j|$.

Homogeneity (hom): Homogeneity measures image homogeneity, and it is sensitive to the presence of near diagonal elements in a GLCM. Therefore, it is calculated by $\mathrm{hom} = \sum_{i=0}^{N_g-1}\sum_{j=0}^{N_g-1}(1/(1+(i-j)^2))\cdot g(i,j)$.

4) Height Characteristics of the Urban Land Cover: In study area 1, the height information obtained from the DSM is combined with other features for the classification of urban land cover. In the experiment, the average relative height of image objects is adopted as a component in the classification for identifying elevated objects, such as buildings, trees, bushes, and lawn.

C. Experiment Design

The analytical procedures of the experiment to determine the significant components that affect the hyperspectral classification result as follows. 1) 14 scenarios for study area 1 were designed with the SVM while 13 scenarios for study area 2. Scenario 1 tests the classification with the spectral component only, and additional scenarios tested the classification with the spectral component and a single spatial component from the set of shape, textural, and height features. Therefore, significant components affecting urban land cover classification can be found. 2) Another 15 and 7 scenarios for study areas 1 and 2, respectively, are designed to test the classification results using different combinations of the component set based on the significant components found in the former experiment. The shape components are first represented by raster images, and the bands transformed from the shape components are combined with the other bands from spectral and textural components for the classification in the following experiments.

D. Correlation Analysis to Exclude Highly Correlated Components

In this section, correlation analysis was used to exclude highly correlated components in our study. Tables V and VI show the results of the correlation matrix for the eight shape components in the two study areas, and Tables VII and VIII show the results of the correlation matrix for the seven textural components in the two study areas. With respect to the shape components, it is assumed that if the two components are highly correlated, then the component with a lower average absolute correlation will be selected for further investigation, along with the rest shape components.

TABLE I
CORRELATION MATRIX FOR EIGHT SHAPE COMPONENTS IN STUDY AREA 1*

	A	*C*	*CX*	*E*	*F*	*RF*	*R*	*S*
A	1.000	-0.478	0.575	-0.145	-0.459	-0.312	-0.306	-0.288
C	-	1.000	-0.704	-0.117	0.942	0.852	0.798	0.883
CX	-	-	1.000	-0.219	-0.662	-0.691	-0.365	-0.749
E	-	-	-	1.000	-0.147	0.231	-0.364	0.159
F	-	-	-	-	1.000	0.772	0.783	0.781
RF	-	-	-	-	-	1.000	0.617	0.937
R	-	-	-	-	-	-	1.000	0.605
S	-	-	-	-	-	-	-	1.000
Average absolute correlation	0.366	0.682	0.566	0.197	0.650	0.630	0.548	0.629

*A: area; C: compactness; CX: convexity; E: elongation; F: form factor; RF: rectangular fit; R: roundness; and S: solidity.

TABLE II
CORRELATION MATRIX FOR EIGHT SHAPE COMPONENTS IN STUDY AREA 2*

	A	*C*	*CX*	*E*	*F*	*RF*	*R*	*S*
A	1.000	-0.465	0.685	0.004	-0.494	-0.132	-0.087	-0.191
C	-	1.000	-0.734	-0.547	0.969	0.552	0.749	0.875
CX	-	-	1.000	0.075	-0.789	-0.322	-0.303	-0.539
E	-	-	-	1.000	-0.487	-0.018	-0.718	-0.375
F	-	-	-	-	1.000	0.495	0.703	0.815
RF	-	-	-	-	-	1.000	0.504	0.723
R	-	-	-	-	-	-	1.000	0.691
S	-	-	-	-	-	-	-	1.000
Average absolute correlation	0.382	0.736	0.556	0.403	0.719	0.468	0.594	0.651

*A: area; C: compactness; CX: convexity; E: elongation; F: form factor; RF: rectangular fit; R: roundness; and S: solidity.

Both Tables I and II show that compactness has high correlation with the form factor, and the correlation coefficients are 0.942 and 0.969, respectively. At the same time, Table I shows that the rectangular fit has high correlation with compactness and solidity, and the correlation coefficients are 0.883 and 0.937, respectively. In Table II, these two correlation coefficients are also significant, which are 0.875 and 0.723, respectively. In addition, Tables I and II show that the form factor has lower average absolute correlation than compactness, and rectangular fit has similar or lower average absolute correlation than solidity. Therefore, six shape components (i.e., area, convexity, elongation, form factor, rectangular fit, and roundness) were chosen for further investigation in the following experiments.

Similarly, according to the results presented in Tables III and IV, the dissimilarity has high correlation with the contrast, and the correlation coefficients are 0.920 and 0.931, respectively.

TABLE III
CORRELATION MATRIX FOR SEVEN TEXTURAL COMPONENTS IN STUDY AREA 1*

	con	*cor*	*dis*	*ene*	*ent*	*hom*	*var*
con	1.000	-0.164	0.920	-0.345	0.501	-0.521	0.847
cor	-	1.000	-0.282	0.230	-0.338	0.276	-0.091
dis	-	-	1.000	-0.484	0.724	-0.645	0.792
ene	-	-	-	1.000	-0.523	0.802	-0.325
ent	-	-	-	-	1.000	-0.354	0.468
hom	-	-	-	-	-	1.000	-0.458
var	-	-	-	-	-	-	1.000
Average absolute correlation	0.614	0.340	0.692	0.530	0.558	0.579	0.569

*con: contrast; cor: correlation; dis: dissimilarity; ene: energy; ent: entropy; hom: homogeneity; and var: variance.

TABLE IV
CORRELATION MATRIX FOR SEVEN TEXTURAL COMPONENTS IN STUDY AREA 2*

	con	*cor*	*dis*	*ene*	*ent*	*hom*	*var*
con	1.000	-0.528	0.931	-0.323	0.608	-0.358	0.783
cor	-	1.000	-0.593	0.254	-0.414	0.361	-0.425
dis	-	-	1.000	-0.404	0.806	-0.344	0.769
ene	-	-	-	1.000	-0.340	0.719	-0.307
ent	-	-	-	-	1.000	0.054	0.584
hom	-	-	-	-	-	1.000	-0.277
var	-	-	-	-	-	-	1.000
Average absolute correlation	0.647	0.511	0.692	0.478	0.544	0.445	0.592

*con: contrast; cor: correlation; dis: dissimilarity; ene: energy; ent: entropy; hom: homogeneity; and var: variance.

The average absolute correlation of contrast is less than that of the dissimilarity. As a result, six textural components (i.e. contrast, correlation, energy, entropy, variance and homogeneity) were chosen for further investigation in the following experiments.

E. Class Separability Analysis to Evaluate Different Components

In the analysis of class separability, the mean (m) and variance (σ^2) of the training samples of each shape and textural component are calculated. Further, the Bhattacharyya distance (B) between a class pair of each component is computed by [54]

$$B_{ij} = \frac{1}{8}(m_i - m_j)^2 \left(\frac{2}{\sigma_i^2 + \sigma_j^2}\right) + \frac{1}{2}\ln\frac{\left|\left(\sigma_i^2 + \sigma_j^2\right)/2\right|}{\sqrt{\sigma_i^2 \sigma_j^2}}. \quad (1)$$

However, the Bhattacharyya distance cannot be directly used for the multiclass feature selection. Therefore, for each component, the minimum Bhattacharyya distance $(\min B)$ among all class pairs representing the distance in the worst case is selected as an indicator for the discriminatory power of the features in the multiclass case [55]. The results of $minB$ for both shape

TABLE V
RESULT OF AVERAGE BHATTACHARYYA DISTANCE FOR SHAPE AND TEXTURAL COMPONENTS IN STUDY AREAS

Component*		*A*	*CX*	*E*	*F*	*RF*	*R*
minB	Study area 1	0.0779	0.0702	0.0073	0.0604	0.0606	0.0552
	Study area 2	0.0045	0.0175	0.0022	0.0348	0.0551	0.0291
Component		*con*	*cor*	*ene*	*ent*	*hom*	*var*
minB	Study area 1	0.0503	0.0014	0.1120	0.1299	0.0703	0.0894
	Study area 2	0.0114	0.0124	0.0399	0.0056	0.0231	0.0072

*A: area; CX: convexity; E: elongation; F: form factor; RF: rectangular fit; R: roundness; con: contrast; cor: correlation; dis: dissimilarity; ene: energy; ent: entropy; hom: homogeneity; and var: variance.

and texture components in study areas 1 and 2 are shown in Table V.

From Table V, we can see that 1) in study area 1, the separability of these components is at an average level of 0.06 [exception cases are a lower value (0.0073) for elongation and two higher values (0.1120 and 0.1299) for energy and entropy], and 2) in study area 2, the component separability is at an average level of 0.02. As a result, a total of six shape components and six texture components were finally used for the following experiments.

IV. RESULTS AND DISCUSSION

A. Result of Finding Significant Components Using SVM

In the experiment, the potential component set included the spectral features, eight shape features, seven textural features and one height feature. Since HyMap data covers 126 bands and ROSIS data covers 103 bands, the training and classification of all spectral bands take a rather long time. Therefore, the spectral components in the experiment are replaced by the first ten principal components of the spectral feature employing principal component analysis [54], and the textural components are analyzed based on the second principal component.

On the basis of the results obtained by excluding highly correlated components, SVM was adopted to test the potential contribution of each component in classifying urban land cover. In the experiments of study areas 1 and 2, 14 scenarios (for study area 1) and 13 ones (for study area 2) was tested: Scenario 1 considers the spectral components only, Scenarios 2 to 7 consider the spectral components and a single-shape component, Scenarios 8 to 13 consider the spectral components and a single textural component, and Scenario 14 considers the spectral components and the height component (only for study area 1). Tables VI and VII present the classification accuracy of these scenarios for each land cover class, as well as the overall accuracy and Kappa coefficient of study areas 1 and 2.

From the results in Table VI, we can see first that in study area 1, among the six shape components, area has the greatest effect on the classification accuracy, increasing the overall accuracy by 2.3%. The convexity, elongation, form factor, and rectangular fit have positive effects on the classification. Roundness has no significant effect on the overall or average accuracy, which decreases the average accuracy slightly while increasing the accuracy for built-up areas by 1.2%. Therefore, we conclude that area, convexity, elongation, form factor, and rectangular fit are suitable shape components for improving the accuracy of classifying urban land cover in study area 1. Second, as far as textural components are concerned, Table VI shows that the contrast is the best textural component in terms of the overall accuracy achievable. Comparing with the other textural components, the correlation, energy, and homogeneity perform relatively poorly in the classification experiment. Third, the mean relative height also has high potential in classifying urban areas, increasing the average accuracy by 2.1% in study area 1.

From the results in Table VII, we can see that first in study area 2, the shape components improve greatly the classification accuracy. All shape components, except rectangular fit, improve the overall classification accuracy by 5.2% to 14.3%. Roundness performs the best among six shape components; the overall classification accuracy reaches 93.3%. Second, for textual components, the overall classification accuracy is beneficial from all textural components, the classification accuracy is increased by 0.6% to 4.4%. At the same time, entropy performs the best among all textual components.

Therefore, based on the above discussion on the experimental results in the two study areas, we can conclude that although the contributions of these components are different, the classification accuracy can be improved generally. However, several components shows different effects on classifying similar urban land cover classes, e.g., rectangular fit improves the classifying accuracy in study area 1, yet decreases the accuracy in study area 2. Homogeneity shows negative effects in study area 1 but improves the accuracy in study area 2. The reason for this trend is the different characteristics of the ground land cover classes and the spatial resolution of the imagery. For example, in study area 1, the buildings are more regular than that of in study area 2. Therefore, rectangular fit works well in study area 1. To investigate how these components affect the classification accuracy, detailed analysis of the impacts of different components on classifying urban land cover classes is discussed in the following section.

B. Effects of Different Components on Classifying Urban Land Cover Classes

1) Classification Tests Using Different Component Sets: Fifteen scenarios for study area 1 and seven scenarios for study area 2 were designed to evaluate the different combinations of the component set for urban land cover classification (see Tables VIII and IX). In the tables, solid circles indicate the component(s) used in the scenarios, while open circles indicate the component(s) not used in the scenario. For instance, ten principal spectral components were used in Scenario 1, and ten principal spectral components and six shape components were used in Scenario 5.

With respect to study area 1, Table VIII shows the following. 1) In Scenarios 1–4, in which a single type of component is used, the spectral components are critical for classifying urban land cover classes. The overall classification accuracy using only spectral components reaches 81.4%, while accuracies using only shape components, only texture components and only height components are 44.5%, 41.4%, and 59.9% respectively. 2) Scenarios 4–10 test different component sets

TABLE VI
CLASSIFICATION ACCURACIES WHEN USING THE SPECTRAL COMPONENTS AND ONE OTHER COMPONENT IN STUDY AREA 1

Component[a] / Accuracy(%)[b]	Only spectra	*A*	*CX*	*E*	*F*	*RF*	*R*	*con*	*cor*	*ene*	*ent*	*hom*	*var*	*HM*
Vegetation	93.6	95.6	91.1	91.7	88.3	87.5	90.8	94.6	93.3	95.4	95.6	98.0	94.6	93.3
Roof	99.5	93.8	92.8	99.4	98.7	99.2	97.7	98.8	99.2	99.5	95.7	98.6	97.8	99.7
Open space	68.8	63.7	62.3	69.9	67.0	63.5	70.6	70.3	69.9	69.7	76.2	73.8	72.0	82.2
Tennis ground	100	100	100	100	100	100	100	100	100	100	100	100	100	100
Road	59.1	71.4	71.5	60.6	69.5	71.3	61.1	63.1	60.0	58.2	60.8	54.6	62.4	56.1
Overall accuracy (%)	81.4	83.7	82.5	81.9	83.3	82.6	81.4	83.7	82.0	81.3	83.4	81.0	83.6	82.2
Kappa	0.75	0.78	0.76	0.76	0.78	0.76	0.75	0.78	0.76	0.75	0.78	0.74	0.78	0.76
Average accuracy (%)[c]	84.2	84.9	83.5	84.3	84.7	84.3	84.0	85.4	84.5	84.6	85.7	85.0	85.4	86.3
Accuracy in build-up areas (%)[d]	76.1	78.6	78.8	77.7	81.1	80.5	77.3	79.0	77.1	75.2	78.1	73.6	78.8	77.4

[a] A: area; CX: convexity; E: elongation; F: form factor; RF: rectangular fit; R: roundness; con: contrast; cor: correlation; dis: dissimilarity; ene: energy; ent: entropy; hom: homogeneity; var: variance; HM: height mean.
[b] Class accuracy: indicates the probability that a sample from land cover map actually matches the reference data and measures the error of commission.
[c] Average accuracy: the average value for all class accuracies.
[d] Accuracy in build-up areas: refers to the classification accuracy except vegetation.

by combining two types of components. Scenario 6 considers textual components and spectral components, and Scenario 7 considers the height component and spectral components, and the overall classification accuracy increased in both cases. 3) Scenarios 11–14 test different component sets by combining three types of components. Scenario 13, which considers spectral, textual, and height components, achieved high classification accuracy (i.e. 84.2%) among all scenarios. 4) Scenario 15 tests the component set using all types of components.

With respect to study area 2, Table IX shows the following. 1) In Scenarios 1–3, in which a single type of component is used, the spectral components are critical for classifying urban land cover classes. The overall classification accuracies using only spectral components, only shape components and only texture components are 79.0%, 83.1%, and 54.7% respectively. 2) Scenarios 4–6 test different component sets by combining two types of components. Scenario 4 considers both shape and spectral components, and Scenario 5 considers both textural and spectral components. Scenario 4 achieves the highest classification accuracy (i.e. 97.8%) when the shape components are accounted for. 3) Scenario 7 tests the component set using all types of components, and it reaches a classification accuracy of 91.7%.

In Table VIII, Scenario 5, which considers all six shape components and the spectra components, decreases the overall accuracy; i.e., the overall classification accuracy in Scenario 5 is lower than that in Scenario 1. Scenario 11, which combines spectral, shape and textural components, also has poor overall classification accuracy. These results are not in accordance with our observation in Section IV-A. The shape components are beneficial for urban land cover classification. The decrease in accuracy might be due to the fact that not all urban land cover classes benefit from inclusion of these shape components (e.g. vegetation areas never have regular size), and using the shape components introduced "noise" into classification, and thus, the overall classification accuracy might decrease when using the shape components. Therefore, the effects of different components on classifying each urban land cover class are further analyzed in the following section.

2) Analysis of the Effects of Different Components on Classifying Urban Land Cover Classes: In the above section, the effect of different components on the classification of urban land cover classes was discussed in terms of the overall accuracy and Kappa coefficient. In this section, the effect of each component on the classification of different urban land cover classes is further analyzed.

From the results of accuracies for each land cover class in study area 1 presented in Tables VI and X, as well as those in study area 2 presented in Tables VII and XI, it can be observed that the effects of the components on the classification of different land cover classes are varied.

For study area 1, we can see the following. 1) Area is the only shape component that improves the accuracy of the vegetation class. The reason is that regions of vegetation have no regular shape and tend to be large. 2) The height component improves the classification accuracy of roofs, achieving an overall accuracy of 99.7%. Moreover, when including the height component, the accuracy for open spaces significantly improves. The accuracy achieved using the height mean is 82.2%, while the classification accuracy without it is 68.8%. 3) Owing to the special spectral characteristic of tennis courts, all scenarios achieve 100% classification accuracy for tennis courts. 4) The inclusion of textual components improves the accuracy of classifying vegetation areas, and the homogeneity is the most significant textual components among the six textual components.

TABLE VII
CLASSIFICATION ACCURACIES WHEN USING THE SPECTRAL COMPONENTS AND ONE OTHER COMPONENT IN STUDY AREA 2

Component[a] / Accuracy(%)[b]	Only spectra	*A*	*CX*	*E*	*F*	*RF*	*R*	*con*	*cor*	*ene*	*ent*	*hom*	*var*
Vegetation	88.8	98.9	91.1	97.2	91.9	85.4	99.2	93.1	88.6	91.7	90.5	90.1	93.3
Roof	68.1	77.7	62.0	80.8	86.8	68.5	87.4	72.4	70.5	85.8	84.2	79.2	71.1
Open space	55.8	81.6	76.8	66.7	80.1	43.3	80.3	62.1	57.2	60.2	61.8	62.0	62.1
Road	95.8	98.7	95.7	95.0	99.3	99.3	99.6	94.7	95.8	92.0	92.6	90.9	94.3
Shadow	100	100	100	100	100	100	100	99.7	100	100	100	100	99.9
Overall accuracy (%)	79.0	91.8	84.2	86.6	90.0	72.2	93.3	82.6	79.6	83.0	83.4	82.6	82.7
Kappa	0.68	0.88	0.76	0.80	0.85	0.60	0.90	0.74	0.69	0.74	0.75	0.74	0.74
Average accuracy (%)[c]	81.7	91.4	85.1	87.9	91.6	79.3	93.3	84.4	82.4	85.9	85.8	84.4	84.1
Accuracy in build-up areas (%)[d]	74.4	83.6	79.0	78.4	91.3	73.0	87.2	75.4	76.0	80.0	81.0	78.6	74.7

[a] A: area; CX: convexity; E: elongation; F: form factor; RF: rectangular fit; R: roundness; con: contrast; cor: correlation; dis: dissimilarity; ene: energy; ent: entropy; hom: homogeneity; var: variance; and HM: height mean.
[b] Class accuracy: indicates the probability that a sample from land cover map actually matches the reference data and measures the error of commission.
[c] Average accuracy: the average value for all class accuracies.
[d] Accuracy in build-up areas: refers to the classification accuracy except vegetation.

For study area 2, we can see the following. 1) Area is the second significant component, which improves the classification accuracy of vegetation. This is consistent with the observations of study area 1. All textual components improve the classification accuracy of vegetation. 2) All shape components, except convexity, improve the classification accuracy of roofs. Energy, entropy, and homogeneity are the most important factors to classify roofs. 3) For the classification of open spaces, shape components (except rectangular fit) are proved to be helpful, while textual components are not. 5) Four shape components, i.e., area, form factor, rectangular fit, and roundness improve the classification of road. 6) Shadow achieves 100% classification accuracy for almost scenarios owing to the low spectral reflectance on all spectral bands.

Fig. 5(a) and (b) shows the variations in accuracies achieved using different components in the classification of four land cover classes (vegetation, roofs, open space, and roads) of study areas 1 and 2. In the figure, the X-axis indicates the components used in the test, and the Y-axis shows the corresponding variation in the classification accuracy for each class.

Fig. 5(a) shows that in study area 1, consideration of area, contrast, energy, entropy, homogeneity, and variance is beneficial in classifying regions of vegetation. The classification accuracy for both roofs and open space is improved using the height component, while the accuracy for roads benefits from inclusion of all the shapes components. Fig. 5(b) shows that in study area 2, the classification accuracies of vegetation and roof are improved by shape and textural components, the classification accuracy of vegetation is improved by area, convexity, elongation, the form factor, roundness, contrast, energy, entropy, homogeneity, and variance, and the classification accuracy of roof is improved by area, elongation, the form factor, roundness, energy, entropy, and homogeneity. Open space is beneficial greatly from area, convexity, the form factor, and roundness, these components improved the classification accuracies by 20% to 26%.

Table X shows that for study area 1, textual components are helpful in classifying vegetation, and the classification accuracies reach 97.6% respectively in Scenario 6 when using both spectral and textural components. The height component is critical to classifying roofs. The classification accuracy for roofs reaches 97.6% when using only the height component in Scenario 4. However, some combinations of different types of components (e.g. Scenarios 5 and 11) achieve lower accuracy than Scenario 1. A possible reason for this is that not all urban land cover classes benefit from consideration of each type of component.

C. Discussions

Based on the analysis of the results obtained from the experiments in the two study areas, several issues are further discussed in this section.

1) Are these multiple features useful for urban land cover classification with airborne hyperspectral data? From the results presented in the above experiments, the answer is yes, that is, multiple features can improve the overall accuracy of classification of land covers. This conclusion can be seen from the experiment results (in Tables VII and VIII) in both study areas. In study area 1, by using the spectral components and one other component, 11 of 13 components improve the overall classification accuracy, and 11 of 12 components improve the overall classification accuracy in study area 2.
2) How should we choose the significant features while they are highly correlated? It is true that from the definitions of the shape and texture features, we can see that some

TABLE VIII
FIFTEEN SCENARIOS TO TEST DIFFERENT COMPONENT SETS* IN STUDY AREA 1

Scenario designing	Spectral components	Shape components	Textural components	Height components	Overall accuracy (%)	Kappa
Scenario 1	●	○	○	○	81.4	0.75
Scenario 2	○	●	○	○	44.5	0.28
Scenario 3	○	○	●	○	41.4	0.22
Scenario 4	○	○	○	●	59.9	0.416
Scenario 5	●	●	○	○	61.8	0.49
Scenario 6	●	○	●	○	84.3	0.79
Scenario 7	●	○	○	●	82.2	0.759
Scenario 8	○	●	●	○	51.0	0.36
Scenario 9	○	●	○	●	51.9	0.38
Scenario 10	○	○	●	●	58.9	0.46
Scenario 11	●	●	●	○	73.9	0.64
Scenario 12	●	●	○	●	64.2	0.53
Scenario 13	●	○	●	●	84.2	0.79
Scenario 14	○	●	●	●	53.7	0.40
Scenario 15	●	●	●	●	83.6	0.78

*●: Component(s) is (are) used in the scenario;
○: Component(s) is (are) not used in the scenario.

TABLE IX
SEVEN SCENARIOS TO TEST DIFFERENT COMPONENT SETS* IN STUDY AREA 2

Scenario designing	Spectral components	Shape components	Textural components	Overall accuracy (%)	Kappa
Scenario 1	●	○	○	79.0	0.68
Scenario 2	○	●	○	83.1	0.74
Scenario 3	○	○	●	54.7	0.39
Scenario 4	●	●	○	97.8	0.97
Scenario 5	●	○	●	86.0	0.79
Scenario 6	○	●	●	89.0	0.83
Scenario 7	●	●	●	91.7	0.88

*●: Component(s) is (are) used in the scenario;
○: Component(s) is (are) not used in the scenario.

of them are correlated. Therefore, in order to find the significant components, correlation analysis needs to be first conducted for these features before the subsequent classification experiment. In our study, for the shape and textual components, it is assumed that if the two components are highly correlated, then the one having a lower average absolute correlation with the other seven ones should be chosen as a significant component. In addition, these features should be further analyzed based on the users' knowledge and experiences.

3) How have these features affected the classification result? From the results in the above experiments, we can see that some features have different impacts on the classification result in the two study areas. For example, in study area 1, roundness has no significant effect on the overall or average accuracy, while in study area 2 roundness performs the best among all the six shape components. The reason responsible for this trend lies in the landscape of the classes of interest. In study area 1, the landscape of the study area is a traditional town, and buildings and roads are more regular than those of in study area 2, which is a university (where buildings are not as regular as those in a traditional city). Therefore, the selection of the significant features should be analyzed based on the understanding of the character-

TABLE X
CLASSIFICATION ACCURACIES OF DIFFERENT COMPONENT SETS FOR DIFFERENT LAND COVER CLASSES IN STUDY AREA 1

Scenario[a] / Class accuracy(%)[b]	1	2	3	4	5	6	7	8	9	10	11	12	13	14	15
Vegetation	93.6	12.6	58.0	43.2	72.6	97.6	93.3	29.0	8.7	63.7	91.4	69.7	97.4	36.2	82.3
Roof	99.5	72.9	53.5	97.6	75.1	93.8	99.7	85.8	95.2	99.3	68.8	95.5	99.2	95.7	96.4
Open space	68.8	8.31	19.9	-	39.3	78.7	82.2	24.1	17.6	28.9	76.2	35.8	84.0	22.6	67.9
Tennis ground	100	26.3	9.6	-	100	100	100	75.0	26.1	22.2	100	100	100	66.3	98.2
Road	59.1	62.5	33.7	-	59.2	61.8	56.1	42.8	65.7	41.1	63.8	58.4	57.6	42.4	76.5
Overall accuracy (%)	81.4	44.5	41.4	59.9	61.8	84.3	82.2	51.0	51.9	58.9	73.9	64.2	84.2	53.7	83.6
Kappa	0.75	0.28	0.22	0.42	0.49	0.79	0.76	0.36	0.38	0.46	0.64	0.53	0.79	0.40	0.78

[a] Scenario: the number of the scenarios in Table IX.
[b] Class accuracy: the probability that a sample from land cover map actually matches the reference data and measures the error of commission.

TABLE XI
CLASSIFICATION ACCURACIES OF DIFFERENT COMPONENT SETS FOR DIFFERENT LAND COVER CLASSES IN STUDY AREA 2

Scenario[a] / Class accuracy(%)[b]	1	2	3	4	5	6	7
Vegetation	88.8	88.8	82.1	99.6	92.7	91.7	98.2
Roof	68.1	76.0	52.0	91.1	84.5	81.8	80.5
Open space	55.8	78.5	47.1	95.8	68.6	91.1	82.2
Road	95.8	81.5	30.1	99.4	91.0	91.2	94.8
Shadow	100	48.9	22.9	100	100	46.3	98.7
Overall accuracy (%)	79.0	83.1	54.7	97.8	86.0	89.0	91.7
Kappa	0.68	0.74	0.38	0.97	0.79	0.83	0.88

[a] Scenario: the number of the scenarios in Table X.
[b] Class accuracy: the probability that a sample from land cover map actually matches the reference data and measures the error of commission.

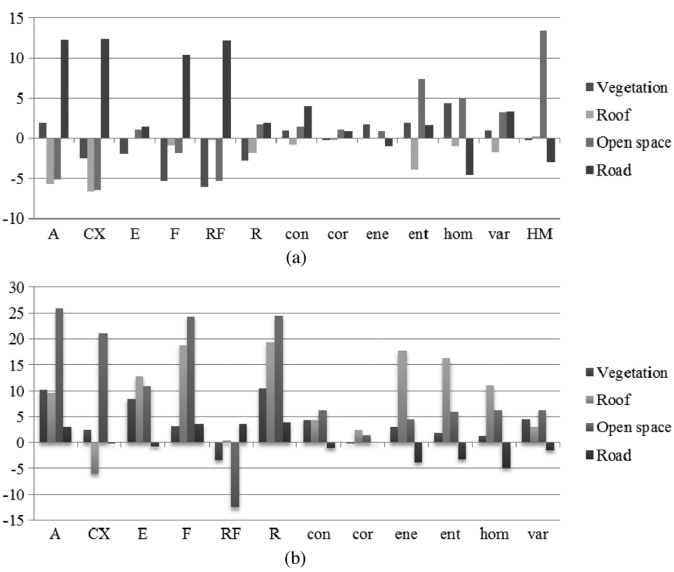

Fig. 5. Accuracy variation due to inclusion of shape and textual components in the two study areas: (a) study area 1 and (b) study area 2.

istics of the classes of interest, such as height information. At the same time, the shape information should be used based on a fine segmentation, in which the shape features of ground objects are correctly presented.

4) The impact of segmentation on the classification result. Segmentation is an important procedure for object-oriented image classification, and fine segmentation result greatly improves the classification accuracy. In particular, the quality of shape features is related to the result of segmentation. As a result, high-quality segmentation is an essential prerequisite for the subsequent classification when using additional shape features.

V. CONCLUSION

This paper investigated the potential effects of spectral, shape, textural, and height components on the classification of urban land cover using remotely sensed hyperspectral data with high spatial and spectral resolutions and determined the combination of components that achieves the highest accuracy in urban classification. Based on the analysis of the spectral, shape, textural, and height characteristics of urban land cover, the spectral component, eight shape components, one height component, and seven textural components were investigated for the potential effects on the classification. A correlation test was first conducted to exclude highly correlated components. Through various experiment scenarios with SVM method, the most significant components affecting the classification were found. The experimental result showed that not all urban land cover classes benefited from inclusion of the shape, textural, or height components in the classification.

The following results were obtained in the experiment.

1) The classification accuracy was higher when significant components from multisource information were utilized.
2) Not all urban land cover classes benefited from the inclusion of all spatial components during classification. The characteristics of each urban land cover type must be considered.
3) Six significant shape components—area, convexity, elongation, the form factor, rectangular fit, and roundness—were found as the most significant components affecting the classification accuracy. Relative height was effective in classifying roofs and open spaces. The texture features were beneficial in classifying certain classes of ground objects such as vegetated areas.
4) Overemphasis of the shape component decreased the overall classification accuracy.

ACKNOWLEDGMENT

The authors greatly appreciate the valuable comments and suggestions of the anonymous reviewers. The authors would like to thank Dr. A. Mueller and Dr. W. Heldens at DLR, Germany, for providing HyMAP data, and Prof. P. Gamba, University of Pavia, for providing ROSIS data.

REFERENCES

[1] F. S. Chapin, III, E. S. Zavaleta, V. T. Eviner, R. L. Naylor, P. M. Vitousek, H. L. Reynolds, D. U. Hooper, S. Lavorel, O. E. Sala, S. E. Hobbie, M. C. Mack, and S. Diaz, "Consequences of changing biodiversity," *Nature*, vol. 405, no. 6783, pp. 234–242, 2000.

[2] I. Douglas, "Hydrological investigations of forest disturbance and land cover impacts in South-East Asia: A review," *Philos. Trans. R. Soc. London B*, vol. 354, no. 1391, pp. 1725–1738, 1999.

[3] D. L. Skole, "Data on global land-cover change: Acquisition, assessment and analysis," in *Changes in Land Use and Land Cover: A Global Perspective*, W. B. Meyer and B. L. Turner II, Eds. Cambridge, U.K.: Cambridge Univ. Press, 1994, pp. 437–471.

[4] P. M. Vitousek, "Beyond global warming: Ecology and global change," *Ecology*, vol. 75, no. 7, pp. 1861–1876, 1994.

[5] G. M. Foody, "Status of land cover classification accuracy assessment," *Remote Sens. Environ.*, vol. 80, no. 1, pp. 185–201, 2002.

[6] D. Lu and Q. Weng, "Urban classification using full spectral information of Landsat ETM+ imagery in Marion county, Indiana," *Photogramm. Eng. Remote Sens.*, vol. 71, pp. 1275–1284, 2005, vol. 11.

[7] M. Herold, X. Liu, and K. C. Clarke, "Spatial metrics and image texture for mapping urban land use," *Photogramm. Eng. Remote Sens.*, vol. 69, no. 9, pp. 991–1001, 2003.

[8] G. M. Foody, "Mapping land cover form remotely sensed data with a softened feedforward neural network," *J. Intell. Robot. Syst.*, vol. 29, no. 4, pp. 433–449, 2000.

[9] P. Watanachaturaporn and M. K. Arora, "Support Vector Machines for Classification of Multi and Hyperspectral Data," in *Advanced Imaged Processing Techniques for Remotely Sensed Hyperspectral Data*, P. K. Varshney and M. K. Arora, Eds. New York, NY, USA: Springer-Verlag, 2004.

[10] B. Haack, N. Bryant, and S. Adams, "An assessment of Landsat MSS and TM data for urban and near-urban land-cover digital classification," *Remote Sens. Environ.*, vol. 21, no. 2, pp. 201–213, 1987.

[11] P. M. Harris and S. J. Ventura, "The integration of geographic data with remotely sensed imagery to improve classification in an urban area," *Photogramm. Eng. Remote Sens.*, vol. 61, no. 8, pp. 993–998, 1995.

[12] W. L. Stefanov, M. S. Ramsey, and P. R. Christensen, "Monitoring urban land cover change: An expert system approach to land cover classification of semiarid to arid urban centers," *Remote Sens. Environ.*, vol. 77, no. 2, pp. 173–185, 2001.

[13] J. R. Anderson, E. E. Hardy, J. T. Roach, and R. E. Witmera, "Land use and land cover classification system for use with remote sensor data," USGS, Washington, DC, USA, U.S. Geological Survey Professional Paper 964, 1976.

[14] M. K. Ridd, "Exploring a V-I-S (vegetation-impervious surface-soil) model for urban ecosystem analysis through remote sensing: Comparative anatomy for cities," *Int. J. Remote Sens.*, vol. 16, no. 12, pp. 2165–2185, 1995.

[15] X. H. Tong, X. Zhang, and M. L. Liu, "Detection of urban sprawl using a genetic algorithm-evolved artificial neural network classification in remote sensing: A case study in Jiading and Putuo districts of Shanghai, China," *Int. J. Remote Sens.*, vol. 31, no. 6, pp. 1485–1504, 2010.

[16] S. E. Franklin and D. R. Peddle, "Classification of SPOT HRV imagery and texture features," *Int. J. Remote Sens.*, vol. 11, no. 3, pp. 551–556, 1990.

[17] P. Gong, D. J. Marceau, and P. J. Howarth, "A comparison of spatial feature extraction algorithms for land-use classification with SPOT HRV data," *Remote Sens. Environ.*, vol. 40, no. 2, pp. 137–151, 1992.

[18] M. A. Shaban and O. Dikshit, "Improvement of classification in urban areas by the use of textural features: The case study of Lucknow city, Uttar Pradesh," *Int. J. Remote Sens.*, vol. 22, no. 4, pp. 565–593, 2001.

[19] O. Debeir, I. Van den Steen, P. Latinne, P. Van Ham, and E. Wolff, "Textural and contextual land-cover classification using single and multiple classifier systems," *Photogramm. Eng. Remote Sens.*, vol. 68, no. 6, pp. 597–605, 2002.

[20] D. J. Marceau, P. J. Howarth, J. M. Dubois, and D. J. Gratton, "Evaluation of the grey-level co-occurrence matrix method for land-cover classification using SPOT imagery," *IEEE Trans. Geosci. Remote Sens.*, vol. 28, no. 4, pp. 513–519, 1990.

[21] J. R. Jensen, *Remote Sensing of the Environment: An Earth Resource Perspective*. Upper Saddle River, NJ, USA: Prentice-Hall, 2000, 544 pp.

[22] S. Bhaskaran, S. Paramananda, and M. Ramnarayan, "Per-pixel and object-oriented classification methods for mapping urban features using Ikonos satellite data," *Appl. Geograph.*, vol. 30, no. 4, pp. 650–665, 2010.

[23] L. Bruzzone and L. Carlin, "A multilevel context-based system for classification of very high spatial resolution images," *IEEE Trans. Geosci. Remote Sens.*, vol. 44, no. 9, pp. 2587–2600, 2006.

[24] A. P. Carleer and E. Wolff, "Urban land cover multi-level region-based classification of VHR data by selecting relevant features," *Int. J. Remote Sens.*, vol. 27, no. 5–6, pp. 1035–1051, 2006.

[25] M. Lackner and T. M. Conway, "Determining land-use information from land cover through an object-oriented classification of IKONOS imagery," *Can. J. Remote Sens.*, vol. 34, no. 2, pp. 77–92, 2008.

[26] M. Herold, D. A. Roberts, M. E. Gardner, and P. E. Dennison, "Spectrometry for urban area remote sensing—Development and analysis of a spectral library from 350 to 2400 nm," *Remote Sens. Environ.*, vol. 91, no. 3–4, pp. 304–319, 2004.

[27] W. G. Cibula and M. O. Nyquist, "Use of topographic and climatological models in a geographical data base to improve Landsat MSS classification for Olympic National Park," *Photogramm. Eng. Remote Sens.*, vol. 53, pp. 67–75, 1987.

[28] P. M. Treitz, P. J. Howarth, and P. Gong, "Application of satellite and GIS technologies for landcover and land-use mapping at the rural—Urban fringe: A case study," *Photogramm. Eng. Remote Sens.*, vol. 58, no. 4, pp. 439–448, 1992.

[29] J. E. Vogelmann, T. Sohl, and S. M. Howard, "Regional characterization of land cover using multiple sources of data," *Photogramm. Eng. Remote Sens.*, vol. 64, pp. 45–57, 1998.

[30] K. Segl, S. Roessner, U. Heiden, and H. Kaufmann, "Fusion of spectral and shape features for identification of urban surface cover types using reflective and thermal hyperspectral data," *ISPRS J. Photogramm. Remote Sens.*, vol. 58, no. 1–2, pp. 99–112, 2003.

[31] H. Buddenbaum, M. Schlerf, and J. Hill, "Classification of coniferous tree species and age classes using hyperspectral data and geostatistical methods," *Int. J. Remote Sens.*, vol. 26, no. 24, pp. 5453–5465, 2005.

[32] M. Voss and R. Sugumaran, "Seasonal effect on tree species classification in an urban environment using hyperspectral data, LiDAR, and an object-oriented approach," *Sensors*, vol. 8, no. 5, pp. 3020–3036, 2008.

[33] A. F. H. Goetz, "Three decades of hyperspectral remote sensing of the Earth: A personal view," *Remote Sens. Environ.*, vol. 113, no. Supp 1, pp. 5–16, 2009.

[34] A. Plaza, J. A. Benediktsson, J. W. Boardman, J. Brazile, L. Bruzzone, G. Camps-Valls, J. Chanussot, M. Fauvel, P. Gamba, A. Gualtieri, M. Marconcini, J. C. Tilton, and G. Trianni, "Recent advances in techniques for hyperspectral image processing," *Remote Sens. Environ.*, vol. 113, no. Supp 1, pp. 110–122, 2009.

[35] B. Waske, S. van der Linden, J. A. Benediktsson, A. Rabe, and P. Hostert, "Sensitivity of support vector machines to random feature selection in classification of hyperspectral data," *IEEE Trans. Geosci. Remote Sens.*, vol. 48, no. 7, pp. 2880–2889, 2010.

[36] C. Small, "Estimation of urban vegetation abundance by spectral mixture analysis," *Int. J. Remote Sens.*, vol. 22, pp. 1305–1334, 2001.

[37] C. Small, "A global analysis of urban reflectance," *Int. J. Remote Sens.*, vol. 26, pp. 661–681, 2005.

[38] M. Herold, M. E. Gardner, and D. A. Roberts, "Spectral resolution requirements for mapping urban areas," *IEEE Trans. Geosci. Remote Sens.*, vol. 41, no. 9, pp. 1907–1919, 2003.

[39] G. Camps-Valls, T. Bandos Marsheva, and D. Zhou, "Semi-supervised graph-based hyperspectral image classification," *IEEE Trans. Geosci. Remote Sens.*, vol. 45, no. 10, pp. 3044–3054, 2007.

[40] Q. Weng and D. Lu, "Landscape as a continuum: An examination of the urban landscape structures and dynamics of Indianapolis city, 1991–2000," *Int. J. Remote Sens.*, vol. 30, no. 10, pp. 2547–2577, 2009.

[41] D. Lua and Q. Weng, "Use of impervious surface in urban land-use classification," *Remote Sens. Environ.*, vol. 102, no. 1–2, pp. 146–160, 2006.

[42] M. E. Hodgson, J. R. Jensen, J. A. Tullis, K. D. Riordan, and C. M. Archer, "Synergistic use of lidar and color aerial photography for mapping urban parcel imperviousness," *Photogramm. Eng. Remote Sens.*, vol. 69, no. 9, pp. 973–980, 2003.
[43] J. A. Benediktsson, J. A. Palmason, and J. R. Sveinsson, "Classification of hyperspectral data from urban areas based on extended morphological profiles," *IEEE Trans. Geosci. Remote Sens.*, vol. 43, pp. 480–491, 2005.
[44] X. Jia, B. C. Kuo, and M. Crawford, "Feature mining for hyperspectral image classification," *Proc. IEEE*, vol. 101, no. 3, pp. 676–697, 2013.
[45] T. Cocks, R. Jenssen, A. Stewart, I. Wilson, and T. Shields, "The HyMap airborne hyperspectral sensor: The system, calibration and performance," in *Proc. 1st EARSeL Workshop Imag. Spectrosc.*, M. E. Schaepman, D. Schlpfer, and D. K. Itten, Eds., EARSeL, Paris, France, 2001, pp. 37–42.
[46] A. Müller, A. Hausold, and P. Strobl, "HySens—DAIS/ROSIS imaging spectrometers at DLR," presented at the SPIE 8th Int. Symp. Remote Sens., Toulouse, France, 2001.
[47] D. J. Robinson, N. J. Redding, and D. J. Crisp, "Implementation of a fast algorithm for segmenting SAR imagery," Australia Defense Sci. and Technol. Org., Scientif. and Tech. Rep., 2002.
[48] T. Blaschke, "Object based image analysis for remote sensing," *ISPRS J. Photogramm. Remote Sens.*, vol. 65, no. 1, pp. 2–16, 2010.
[49] B. M. Mehtre, M. S. Kankanhalli, and W. F. Lee, "Shape measures for content based image retrieval: A comparison," *Inf. Process. Manag.*, vol. 33, no. 3, pp. 319–337, 1997.
[50] N. Mohanty, T. M. Rath, A. Lee, and R. Manmatha, "Learning shapes for image classification and retrieval," *Lecture Notes Comput. Sci.*, vol. 3568, pp. 589–598, 2005.
[51] J. C. Russ, *The Image Processing Handbook*, 4th ed. Boca Raton, FL, USA: CRC Press, 2002.
[52] R. M. Haralick, K. Shanmugam, and I. Dinstein, "Textural features for image classification," *IEEE Trans. Syst. Man. Cybern.*, vol. SMC-3, no. 6, pp. 610–621, 1973.
[53] A. Baraldi and F. Parmiggiani, "An investigation of the textural characteristics associated with gray level cooccurrence matrix statistical parameters," *IEEE Trans. Geosci. Remote Sens.*, vol. 33, no. 2, pp. 293–304, 1995.
[54] S. Theodoridis and K. Koutroumbas, *Pattern Recognition*. New York, NY, USA: Academic, 2003.
[55] S. Gunal and R. Edizkan, "Subspace based feature selection for pattern recognition," *Inf. Sci.*, vol. 178, no. 19, pp. 3716–3726, 2008.

Xiaohua Tong received the Ph.D. degree from Tongji University, Shanghai, China, in 1999.

He worked as a Postdoctoral Researcher in the State Key Laboratory of Information Engineering in Surveying, Mapping, and Remote Sensing, Wuhan University, China, between 2001 and 2003. He was a Research Fellow in The Hong Kong Polytechnic University in 2006, and a visiting scholar at the University of California, Santa Barbara, CA, USA, between 2008 and 2009. His current research interests include remote sensing, GIS, uncertainty and spatial data quality, image processing for high resolution, and hyperspectral images.

Dr. Tong serves as the Vice-Chair of the Commission on Spatial Data Quality of the International Cartographical Association, and the Co-Chair of the ISPRS working group (WG II/4) on Spatial Statistics and Uncertainty Modeling.

Huan Xie received the B.S. degree in surveying engineering and the M.S. and Ph.D. degrees in cartography and geoinformation from Tongji University, Shanghai, China, in 2003, 2006, and 2009, respectively.

From 2007 to 2008, she was a visiting student at the Institute of Photogrammetry and GeoInformation, Leibniz Universität, Hannover, Germany, under the support of the China Scholarship Council (CSC) Scholarship. Since June 2009, she has been working in the College of Surveying and Geo-Informatics, Tongji University. She is currently a Lecturer and teaches courses related to remote sensing and GIS. Her research interests include hyperspectral remote sensing and polar remote sensing.

Qihao Weng received the Ph.D. degree from the University of Georgia, Athens, GA, USA, in 1999.

He is a Professor in the Department of Geography, Geology, and Anthropology at Indiana State University, Terre Haute, IN, USA. His expertise includes remote sensing, GIS, and environmental modeling, with an application concentration on urban ecosystems and land use and land cover change. He has published more than 100 refereed journal articles and book chapters.

Dr. Weng is an Associate Editor of the *ISPRS Journal of Photogrammetry and Remote Sensing* and the series editor for both the Taylor & Francis Series in Remote Sensing Applications and the McGraw-Hill Series in GIS&T. He was the recipient of 1999 Robert E. Altenhofen Memorial Scholarship Award by the American Society for Photogrammetry and Remote Sensing. In 2006, he received the Theodore Dreiser Distinguished Research Award by Indiana State University, and in 2008, he was awarded a senior fellowship from NASA.